Hindawi
Advances in Civil Engineering
Volume 2020, Article ID 8822955, 16 pages
https://doi.org/10.1155/2020/8822955

Research Article

Performance-Based Seismic Fragility and Residual Seismic Resistance Study of a Long-Span Suspension Bridge

Fangwen Wu,[1] **Jianfei Luo**,[1] **Wei Zheng**,[1] **Cheng Cai**,[1] **Jun Dai**,[1] **Yajun Wen**,[1] **and Quanyou Ji**[2]

[1]*School of Highway, Chang'an University, Xi'an 710064, China*
[2]*China Coal Xi'an Design Engineering Co. Ltd., Xi'an 710054, China*

Correspondence should be addressed to Fangwen Wu; wufangwen2004@163.com

Received 10 April 2020; Revised 2 September 2020; Accepted 18 September 2020; Published 30 September 2020

Academic Editor: Agathoklis Giaralis

Earthquakes can cause serious damage to traffic infrastructure and even induce the collapse of bridges, which is even worse. At the same time, earthquakes are key factors to the overall service capacity of the traffic network. Therefore, mastering the failure mechanism and evaluating accurate residual seismic resistance of a bridge under earthquakes are of great significance to the rapid recovery of traffic network function. For this reason, a performance-based methodology for the evaluation of the residual seismic resistance of a suspension bridge is proposed. In this paper, we provide the fragility curves of the key sections of the pier by incremental dynamic analysis (IDA), mathematical statistical analysis, and the damage law and obtained the failure state of the structure and the overall seismic capacity residual ratio and the stage seismic capacity residual ratio of the structure. Then, based on the research results of IDA, the reserve seismic capacity is analyzed as well. The research results explore a new method to accurately estimate the residual seismic capacity for resilience assessment.

1. Introduction

In recent years, earthquakes have occurred frequently all over the world, causing serious damage to building structures, making earthquake resilience one of the key issues in the field of engineering [1–3]. Seismic resilience means the ability of a structure to recover its functions after an earthquake [4]. It was a new concept proposed by Bruneau to evaluate the resilience of a community after an earthquake, and later, the idea was applied to the field of civil engineering [5]. Determining the residual seismic capacity of a bridge is the key to study seismic resilience.

Over the past decades, suspension bridges, which are associated with exquisite shape and lightweight configuration, are widely used to adapt to objective traffic conditions and supply effective traffic operations in modern infrastructure [6–9]. It is generally considered that the seismic performance of suspension bridges is better than that of cable-stayed bridges and continuous rigid-frame bridges. Actually, their working performance has not been well understood yet due to complex mechanical structure and the lack of evaluation methods. In recent studies, a series of numerical simulations and theoretical and methodological investigations have been carried out to investigate this issue in the world.

Numerical simulation of bridges often analyzes the relationship between the deterioration of materials and their recoverability. For instance, Casciati et al. numerically analyzed the concept of seismic resilience of a cable-stayed bridge and a strategy for recovering the optimal configuration of the bridge after suffering a damaging event [10]. Amir and Devin introduced the finite element method to analyze the performance of other in-service bridges degraded under the effect of different damaging scenarios, which provided the possibility to determine a measure of capacity, resilience, and remaining service life [11]. Vishwanath and Banerjee numerically analyzed the resilience of the deteriorating reinforced concrete (RC) bridge under seismic ground motions (GMs) and found a degrading trend of resilience of the bridge as it ages [12].

Appropriate theories and methods are also the basic prerequisites for fruitful results. Therefore, numerous research studies, about evaluation of the seismic capacity of the bridge, have been conducted. For instance, Dong proposed a probabilistic framework for assessing the risk and resilience of a bridge suffering from major shock and aftershocks while incorporating its uncertainties [13]. Decò et al. used the six-parameter sinusoidal-based recovery model [14]. Bocchini and Frangopol put forward an optimal cost recovery identification method, which could automatically identify the most critical bridge in the transportation system and calculate the optimal recovery scheme based on available funds [15]. Alicia carried out the experiment of RC columns and CFFT columns, and from that, the residual axial load-carrying capacities of them were obtained. They also estimated restoration time and repair cost for each type of column [16]. Hazus developed restoration curves for highway bridges that had the functional form of a normal cumulative distribution function [17].

All these research studies have greatly promoted the application of seismic reliance of bridges. However, there are still some tough problems which have been puzzling researchers and restricting the development of this field. (1) As is known to all, the response mechanism of different bridge structures under an earthquake varies greatly. Although numerous theories and methods were proposed in the past years, they have not yet achieved an accurate method for the seismic residual capacity under different earthquake intensities for suspension bridges with asymmetric towers even for simply supported beam bridges [17]. While the structure is undergoing restorable repair, this situation directly leads to overuse of materials and excessive economic costs in engineering applications. (2) The information about earthquakes cannot be predicted before they occur. Thus, many researchers have selected the largest seismic waves in the history of the structure location to evaluate the seismic response of bridges. It is difficult to know the expected residual seismic value of bridge structures, and the performance of bridges cannot be evaluated rapidly and accurately after different earthquakes.

Following the aforementioned extensive review, many researchers just studied the seismic responses of bridges to earthquakes. However, until now, no researcher has studied the residual seismic resistance of the long-span bridge with asymmetrical suspension bridges. Hence, the purpose of this paper is to provide a method to quantify the residual seismic resistance of asymmetrical suspension bridges, which can not only assess the overall seismic residual capacity but also the seismic residual capacity in stages. First, the fragility is studied in detail by the incremental dynamic analysis method and mathematical statistics. Then, according to the damage state, the indexes of overall recoverability and stage recoverability are established. Finally, the expected residual ratio of aseismic capability under three different seismic intensities is analyzed. The method proposed in this paper is based on the analysis of the performance of the bridge. Compared with other restorability assessment methods, the seismic residual capacity of the bridge under different earthquake intensities can be quantified. It is of great significance to the design, construction, and recoverability analysis of bridges.

2. Methods and Theories

2.1. Method of Incremental Dynamic Analysis. Incremental dynamic analysis (IDA) is a useful tool to evaluate the performance of structures against seismic actions. In this, the recorded ground motion is magnified according to the calculation requirements, and the external load acts on the finite element model; then, the response value of the finite element model under the action of the nonlinear time history is obtained [18].

2.2. Fragility Function Methodology. Analytical fragility functions have been widely used in recent years because of their characteristics of flexibility and accuracy [19, 20]. It is also a useful tool to evaluate the probability of a certain limit state or conditional probability and the basis for resilience. The results of fragility functions can be expressed by fragility curves [21, 22].

Analytical fragility curves can be developed in three ways, which are known as the statistical method, regression analysis, and capacity demand ratio. Each of the three methods has its own advantages. The method of capacity demand ratio is adopted because of its accuracy in this study: it uses the scaling approach for intensity measure (IM) and evaluates specific engineering demand parameters (EDP) so that IDA has been performed by scaling and applying the selected accelerograms [23]. The fitting curve is expressed as follows:

$$\begin{aligned} \mathrm{DI} &= A[\ln(\mathrm{IM})]^2 + B[\ln(\mathrm{IM})] + C, \\ \sigma &= \sqrt{\frac{S_r}{(n-2)}}, \\ P_f &= P\left[\frac{S_d}{S_{\mathrm{ci}} > 1}\right] = 1 - \Phi\left[\frac{\ln(1) - \mu}{\sigma}\right] = \Phi\left(\frac{\mu}{\sigma}\right), \end{aligned} \tag{1}$$

where DI is the seismic demand; IM is the intensity measure; A, B, and C are the regression parameters; σ is the standard deviation; S_r is the residual sum of squares; n is the sample number; P_f is the damage probability; S_d is the demand of structural response; S_{ci} is the damage index; μ is the mean value.

2.3. Damage Index. The key to seismic fragility analysis is to determine the performance target of the structure and quantify the damage state. According to the assessment method of section damage, researchers put forward the park index, capability demand index, crack index, displacement ductility index, and curvature ductility index. These five indices can be used to quantitatively analyze structural damage.

The curvature ductility index is more accurate for high-rise structures, such as suspension bridges [24, 25]. Hence, the curvature ductility index is adopted in this study. Here,

there are five types of damaged states in the key section: nondamaged, slightly damaged, mud damaged, severely damaged, and completely damaged. The critical curvature is defined as $\varphi_1, \varphi_2, \varphi_3$, and φ_4, respectively, and information is shown in Table 1 [26]. The main steps are as follows:

First, the axial force and bending moment of the key sections of the tower under the most unfavorable load combination are calculated using the numerical model. Then, by analyzing bending moment and curvature, the relationship between bending moment and curvature is obtained. Finally, the damage range of the section is divided by the relation between the section bending moment curvature and the strain limit of the material. The interval positions of the defined damage states are shown in Figure 1.

2.4. Seismic Resilience Index. As is shown in Figure 2, the curve can reflect the evolution process of nonlinear attenuation of the seismic resistance of the structure from the intact state to complete damage. Its expression is as follows:

$$C(D) = \frac{\mathrm{IM_{Di}}}{\mathrm{IM}}, \tag{2}$$

where $C(D)$ represents the residual ratio of the seismic capacity of the structure when the damage value is D; $\mathrm{IM_{Di}}$ represents the residual seismic capacity corresponding to the structural damage of D; IM is the intensity measure (when $D = 0$).

In performance-based seismic research, the overall seismic resilience index can be used to evaluate the seismic capability of the structure macroscopically, but it is not suitable to classify the seismic capability of the structure step by step. In view of the problem that the recoverability of the structure in different damaged states cannot be quantified, this study proposes the seismic recoverability index of the structure at different stages, and its expression is as follows:

$$I_{\mathrm{Di}} = \frac{\int_{D_i}^{D_{i+1}} C(D)\mathrm{d}D}{D_{i+1} - D_i}, \tag{3}$$

where I_{DI} is the index of recoverability; D_{i+1} and D_i are the corresponding residual seismic ultimate ratios within the adjacent damaged intervals.

2.5. Assessment of the Seismic Residual Capacity. According to the seismic fragility analysis, the probability of different degrees of damage to the section of the main tower under the excitation of the arbitrary ground motion intensity level is obtained, and the probability of occurrence of each damaged stage under the action of a specific intensity earthquake is obtained through the method of conditional probability statistical analysis, as shown in the following equation:

$$P(D_i) = \begin{cases} 1 - P(D_{i+1}), & i = 0, \\ P(D_i) - P(D_{i+1}), & 0 < i < 4, \\ P(D_i), & i = 4, \end{cases} \tag{4}$$

where $P(D_i)$ is the probability of different damage states.

As shown in equation (4), the probability of different damaged stages depends upon the specific ground motion intensity, and the expected value E_{IM} of the seismic resistance residual ratio of the key section of the bridge's main tower under the action of specific ground motion intensity grade IM is obtained by combining it with I_{Di}, the recoverable index in the structural stage, as shown in the following equation [26]:

$$E_{\mathrm{IM}} = \sum_{i=0}^{4} P(D_i) \cdot I_{\mathrm{Di}}. \tag{5}$$

3. Engineering Application

3.1. Investigated Bridge. The Puli Bridge in Yunnan Province of China, an earth-anchored suspension bridge with a span of 166 + 628 + 166 m, is illustrated as an example in this study. The overall layout of the bridge is presented in Figure 3(a).

The main cable consists of 91 prefabricated parallel steel wire bundles with a transverse distance of 26 m, and the rise-span ratio is 1/10. There are 50 pairs of suspension cables in the whole bridge. The standard spacing is 12 m. As is shown in Figure 3(b), the cable tower is made of reinforced concrete with the height of left and right legs of 153.5 m and 138.5 m, respectively. In addition, it is made of C50 concrete. In Figure 3(c), the girder is 3 m in height with 2% cross slope and 28.5 m in width. It is made of low-alloy high-strength structural steel. Detailed information is available in the literature [27].

In order to reveal the seismic behaviour of the long-span suspension bridge with legs of different heights and study the residual seismic capacity, this work determines the key sections according to the principle of frail section and equal interval. As shown in Figures 3(b) and 3(d), six key sections are taken from the left and right legs of the main tower, respectively.

3.2. Analysis of the Bridge. The earth-anchored suspension bridge model is constructed using finite element software SAP 2000 [28]. In order to simulate the bridge accurately, a large number of references are consulted [29–36]. In the finite element analysis, the three-dimensional finite element model is established according to the structural characteristics of the suspension bridge. Both the girder and the main tower adopt the space beam element, in which the girder adopts the single girder to carry on the simulation. The second stage of constant load is mainly simulated by distributed mass. The main cable and derrick are simulated by the cable element. According to the design cable force and material parameters provided by the design unit, the overall cooling method is adopted to apply tension. The bottom of the tower and the end of the main cable, both, are fixed end constraints. The connection stiffness between each tower pier and the main beam is applied according to the specified stiffness value provided by the design unit. The main vibration modes are shown in Figure 4.

Table 1: Characteristics of the curvature ductility index.

Damage status	Damage characteristics	Specific parameter index
Nondamaged	The outermost longitudinal reinforcement is not yielded	$\varphi_s \le \varphi_y$
Slightly damaged	The yield strain of the outermost longitudinal bars is less than the initial strain, and the compressive strain of unconstrained concrete is less than 0.004	$\varphi_y < \varphi_s \le \varphi_{sh}$, $\varphi_c \le 2\varphi_{co}$
Mid damaged	The longitudinal reinforcement strain is less than 0.55 times of the ultimate tensile strain, and the constrained concrete is less than 0.75 times of the ultimate compressive strain	$\varphi_{sh} < \varphi_s \le 0.55\varphi_{su}$, $2\varphi_{co} < \varphi_c \le 0.75\varphi_{cc}$
Severely damaged	The longitudinal reinforcement strain is less than the ultimate tensile strain, and the constrained concrete is not larger than the ultimate compressive strain	$0.55\varphi_{su} < \varphi_s \le \varphi_{su}$, $0.75\varphi_{cc} < \varphi_c \le \varphi_{cc}$
Completely damaged	The longitudinal reinforcement strain is greater than the ultimate tensile strain and the restrained concrete cracks	$\varphi_s > \varphi_{su}$, $\varphi_c > \varphi_{ccu}$

where φ_s represents the tensile strain of the outermost longitudinal reinforcement of the section; φ_c represents the compressive strain of unconstrained concrete on the outermost side of the cross section; φ_y represents the theoretical yield strain of longitudinal reinforcement; φ_{cc} represents the compression strain of the outermost constrained concrete of the section; φ_{co} represents the strain corresponding to the peak compressive stress of unconstrained concrete; φ_{sh} represents the tensile strain when the longitudinal reinforcement is initially hardened; φ_{ccu} represents the tensile strain of the outermost constrained concrete of the section.

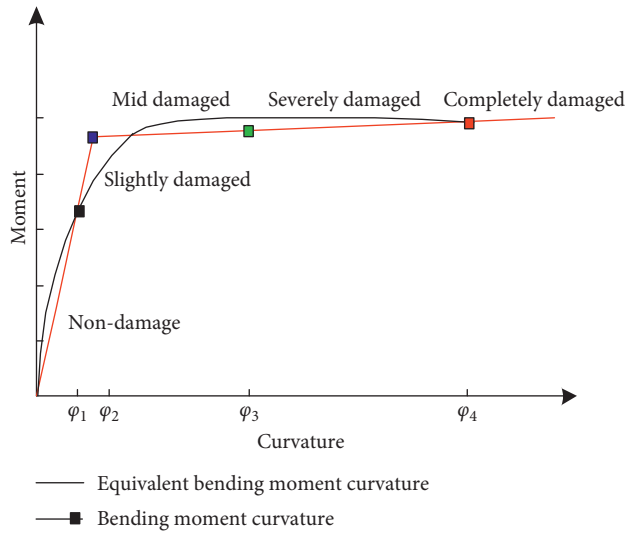

Figure 1: Schematic diagram of the damage state interval.

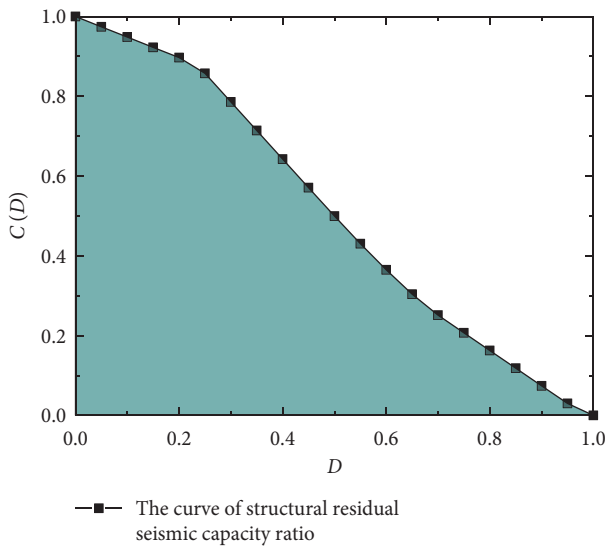

Figure 2: The curve of the structural stage residual seismic capacity ratio.

3.3. Selection of Ground Motions. To establish a probabilistic model based on the measured data obtained from nonlinear dynamic analysis, an appropriate ground motion record should be selected [2, 37]. As mentioned by general rules [22], the ground motion bin should contain sufficient information about the strength and structural characteristics of the earthquakes. Each selected ground motion record should be independent of the type of structure and applicable to a variety of structures at different locations. In addition, the number of records should be large enough to cover seismic variability in a reasonable way. Previous studies have shown that 12 ground motions can provide sufficient precision in the estimation of seismic demands [38, 39].

According to the mentioned objectives, the seismic waves with good applicability are selected. The seismic waves used in this study were selected from the ground motion database of the Pacific Earthquake Engineering Research Center and processed by seismic signals. From the calculation of the dynamic characteristics of the structure, it is known that the first-order vibration mode is a positive symmetrical transverse bending, so this study analyzes and calculates the lateral ground motion of the bridge structure. According to the Chinese standard JTG/T D65-05 (2015) [40], the damping ratio of the suspension bridge is determined as 2%, and then, the intensity index of ground motion Sa ($T1 = 6.64$ s, $\xi = 2\%$) is calculated.

In order to meet the needs of IDA calculation, seismic waves are divided into 10 grades from small to large. The selected seismic waves are shown in Table 2, the classification of ground motion intensity is shown in Table 3, and the amplitude modulation coefficient of seismic waves is shown in Table 4.

4. Analytical Results and Discussions

4.1. The Results of Incremental Dynamic Analysis. The seismic responses of the key sections of the piers are obtained through the calculation results of IDA. Figure 5 shows the IDA curves of each section of the main tower. By comparing the IDA curves of 10 key sections of the left and right legs of

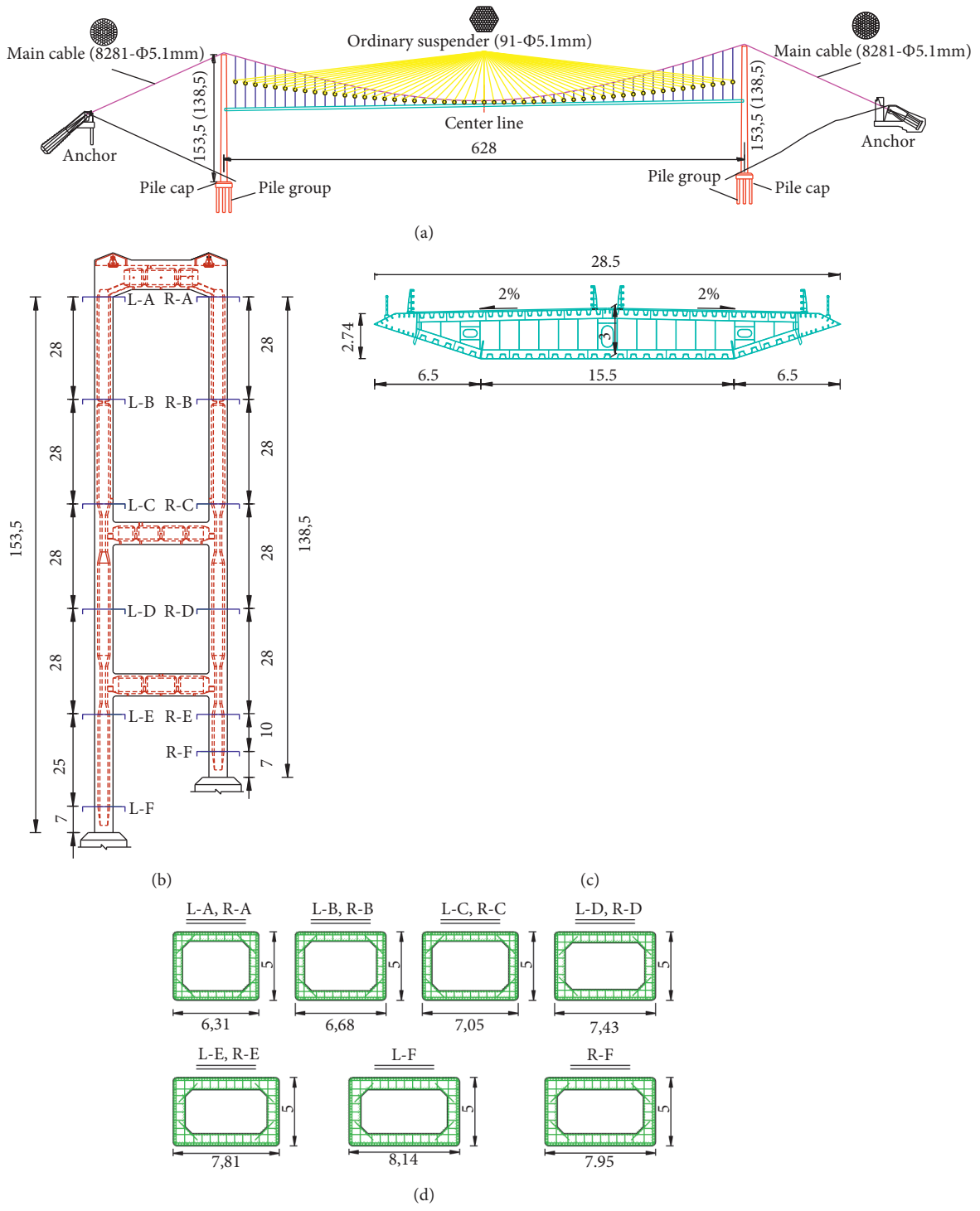

FIGURE 3: Puli Bridge. (a) A general view of the bridge. (b) Photos of the tower. (c) Cross section of the deck. (d) Cross section of the tower (units: m).

the main tower, it can be concluded that the section curvature is obviously different under different earthquakes; especially, section A, section C, and section F are sensitive to earthquakes. The seismic performance is also relatively weak. In addition, under the action of the earthquake, the response of the key sections of the right leg is more sensitive than that of the left leg.

4.2. The Results of Fragility Analysis. According to the results of seismic performance by the method of IDA in this study, the probability of various damages to key sections of piers under the action of the longitudinal bridge to the ground is obtained. Based on the method of obtaining seismic vulnerability curves, the seismic vulnerability curves of 12 sections with different damages are drawn in Figure 6.

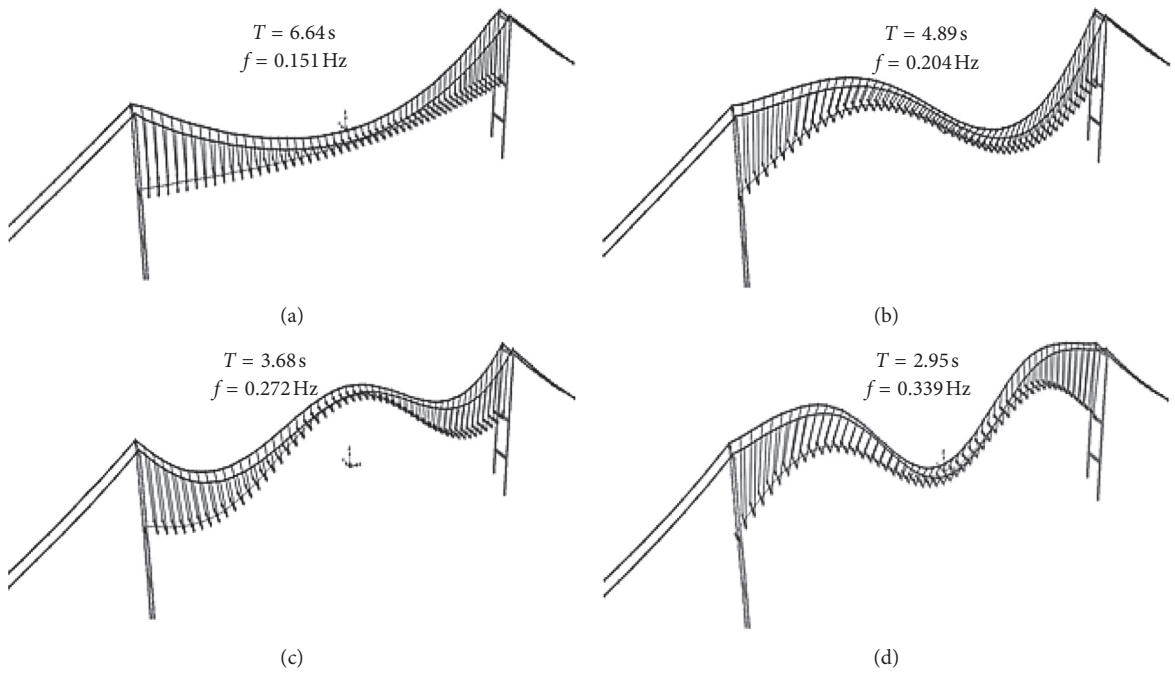

Figure 4: The dimensional model of the Puli Bridge in SAP2000. (a) First-order vibration mode. (b) Second-order vibration mode. (c) Third-order vibration mode. (d) Fourth-order vibration mode.

Table 2: Characteristics of the earthquake ground motion histories.

ID no.	Year	Event	Station	PGA (g)	*Sa* (*T*1) (g)	Duration (s)
1	2013	LS, China	Lushan	1.026	0.0121	5.7
2	2008	WC, China	Wolong	0.978	0.0075	29.5
3	1999	CHI-CHI, China	TCU045	0.361	0.0251	11.8
4	1999	Kocaeli	YARIMCA	0.35	0.0900	15.8
5	1995	Kobe, Japan	KAKOGAWA	0.345	0.0218	13.2
6	1994	Northridge, America	CDMG 24278	0.568	0.0245	8.9
7	1992	Landers, America	SCE 24	0.78	0.1202	15.4
8	1989	Loma Prieta, America	CDMG 47381	0.367	0.0324	11.62
9	1983	Trinidad	CDMG 1498	0.194	0.0081	8.0
10	1979	Imperial Valley	USGS 5115	0.315	0.0396	8.4
11	1976	Friuli, Italy	TOLMEZZO	0.351	0.0082	4.2
12	1961	Hollister, America	USGS 1028	0.195	0.0087	16.3

Table 3: Classification of ground motion intensity.

Magnitude of the earthquake	*Sa* (*T*1) (g)
1	0.009
2	0.018
3	0.027
4	0.036
5	0.045
6	0.054
7	0.063
8	0.072
9	0.081
10	0.090

From Figure 6, it can be concluded that the damage probability of the right leg of the tower column with the same position key section is higher than that of the corresponding section of the left leg of the tower column under the same damage state. Thus, it indicates that, in the case of towers with legs of unequal heights, the one with shorter height has more damage probability among its key sections. The damage probability of section A, section C, and section F increases rapidly with the ground motion strength, and the damage probability is larger. These sections should be fully considered in seismic design.

4.3. Analysis of Integral and Stage Seismic Resistance. Based on the abovementioned analysis results of the Puli Bridge, it can be concluded that section A, section C, and section F on the right leg of the main tower entered into a state of complete damage under the action of multiple earthquakes. Therefore, seismic resilience analysis is carried out on these sections. The residual ratio of seismic capability corresponding to each section was averaged and plotted in the plane Cartesian coordinate system, and then, the overall

Table 4: Seismic waves amplitude modulation coefficient.

M	1	2	3	4	5	6	7	8	9	10
Wave 1	7.3	14.6	21.8	29.1	36.4	43.7	51.0	58.3	65.5	72.8
Wave 2	11.8	23.5	35.3	47.0	58.8	70.6	82.3	94.1	105.8	117.6
Wave 3	3.5	7.0	10.5	14.0	17.6	21.1	24.6	28.1	31.6	35.1
Wave 4	1.0	2.0	2.9	3.9	4.9	5.9	6.9	7.8	8.8	9.8
Wave 5	4.0	8.1	12.1	16.2	20.2	24.3	28.3	32.4	36.4	40.5
Wave 6	3.6	7.2	10.8	14.4	18.0	21.6	25.2	28.8	32.4	36.0
Wave 7	0.7	1.5	2.2	2.9	3.7	4.4	5.1	5.9	6.6	7.3
Wave 8	2.7	5.4	8.2	10.9	13.6	16.3	19.0	21.8	24.5	27.2
Wave 9	10.9	21.8	32.7	43.6	54.5	65.4	76.3	87.2	98.1	109.0
Wave 10	2.2	4.5	6.7	8.9	11.1	13.4	15.6	17.8	20.0	22.3
Wave 11	10.8	21.5	32.3	43.0	53.8	64.5	75.3	86.0	96.8	107.6
Wave 12	10.1	20.3	30.4	40.6	50.7	60.8	71.0	81.1	91.2	101.4

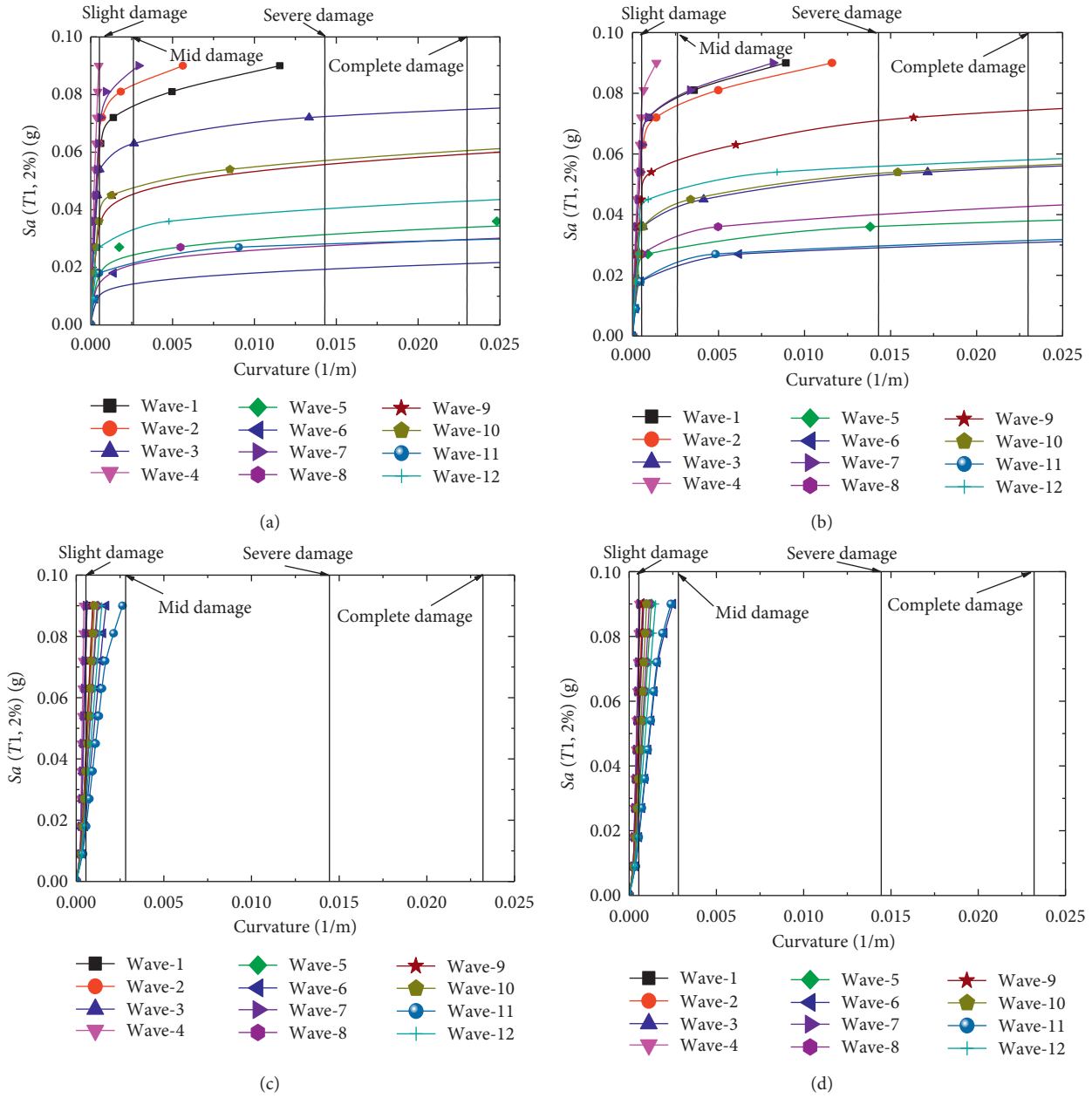

Figure 5: Continued.

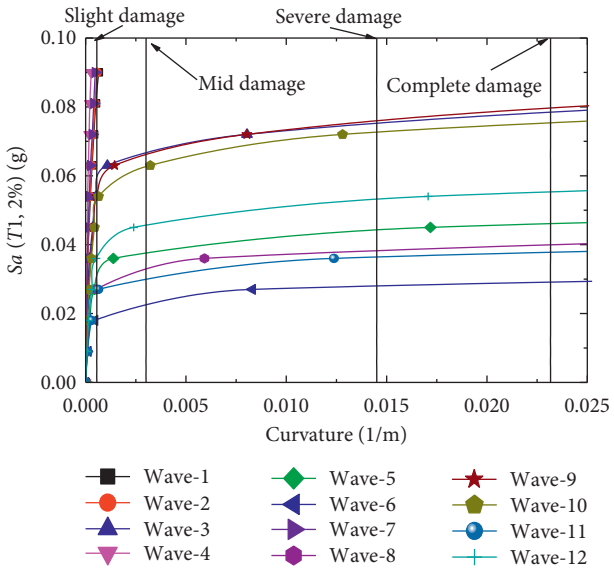

(e)

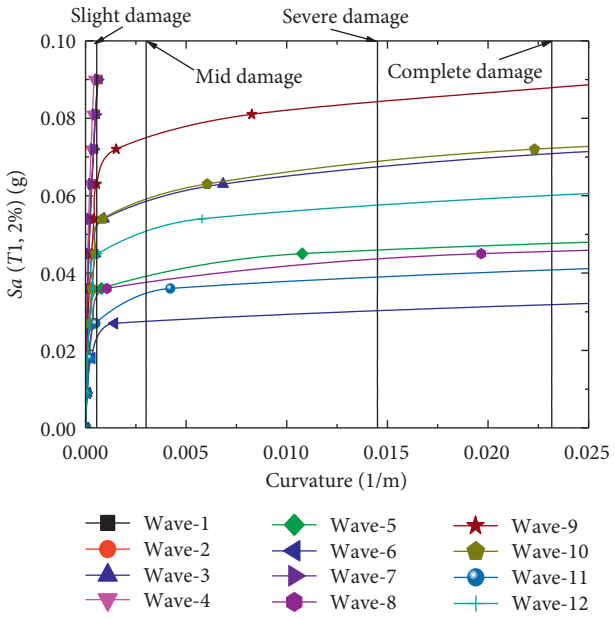

(f)

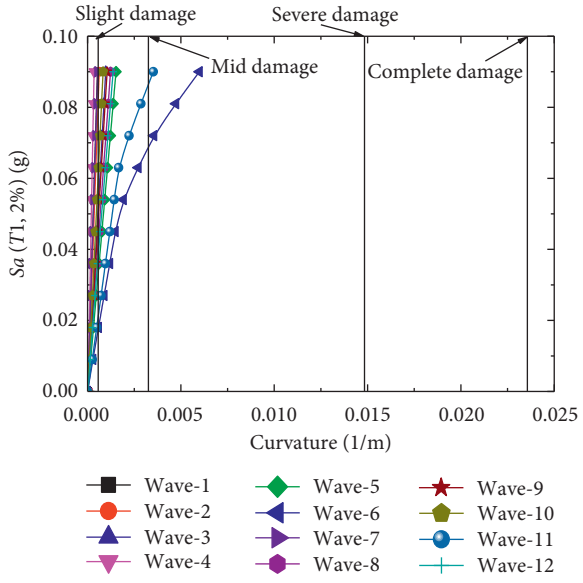

(g)

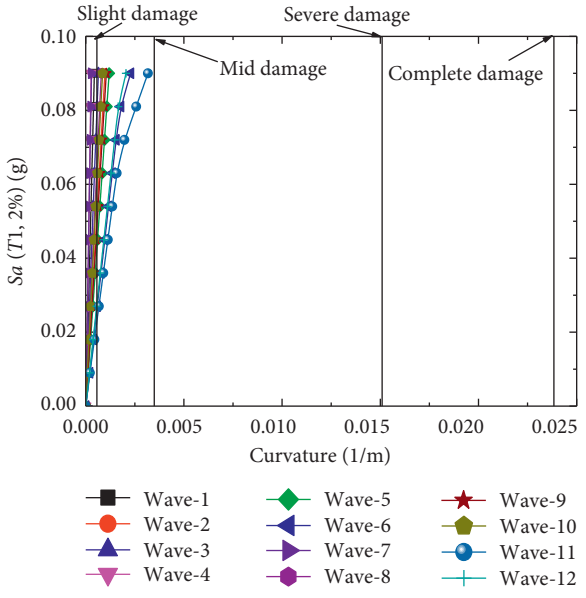

(h)

Figure 5: Continued.

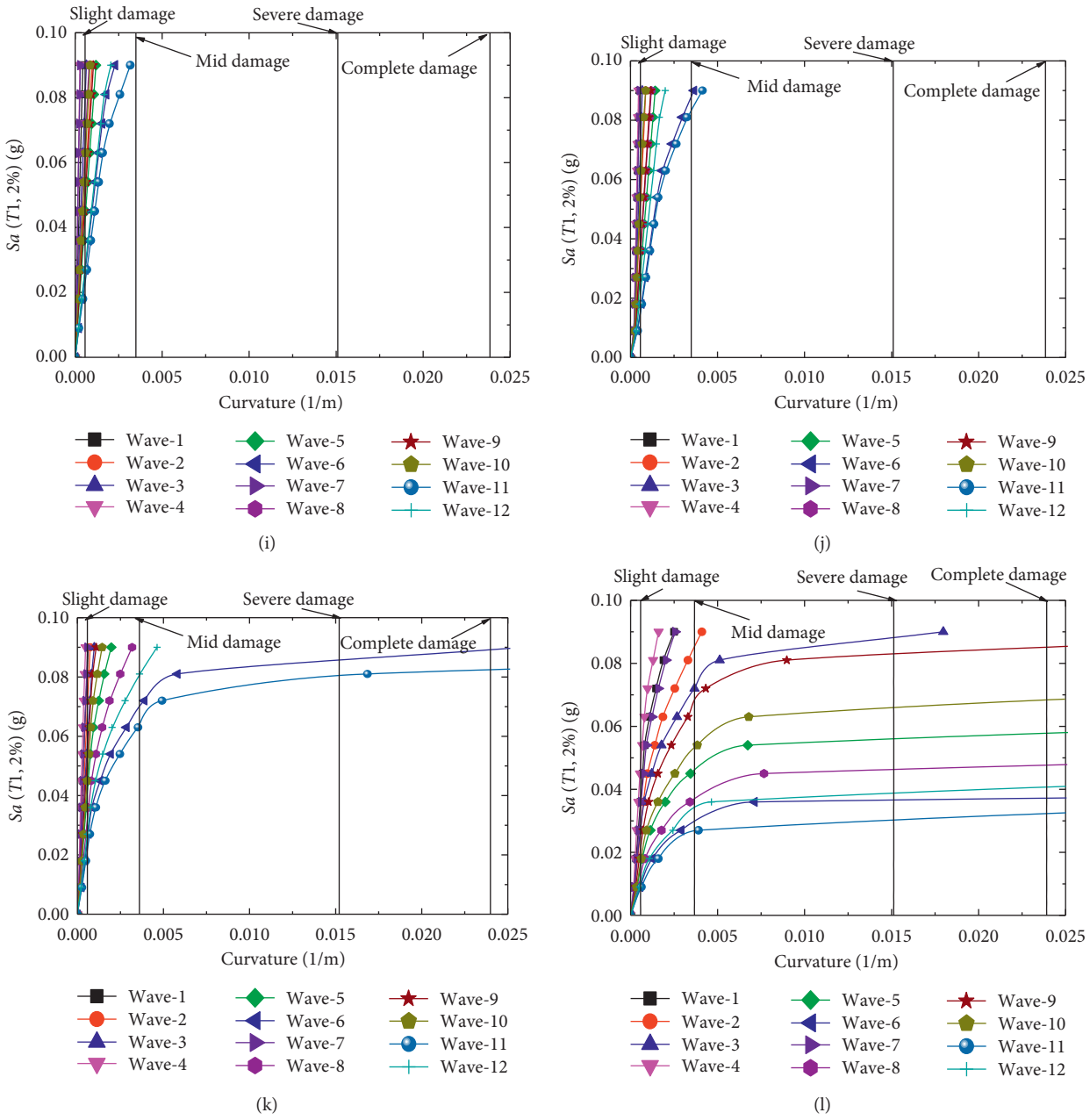

Figure 5: The IDA curve of the Puli Bridge. (a) Section L-A. (b) Section R-A. (c) Section L-B. (d) Section R-B. (e) Section L-C. (f) Section R-C. (g) Section L-D. (h) Section R-D. (i) Section L-E. (j) Section R-E. (k) Section L-F. (l) Section R-F.

residual ratio curve of seismic capability of the key section was obtained. Taking section R-A as an example, the mean value of the R-A section's seismic capacity residual ratio was calculated, the overall seismic capacity residual ratio curve of section R-A was drawn, and the overall seismic resilience index of 0.5352 was obtained. The same method was used to obtain the overall seismic capacity residual ratio curve of sections R-C and R-F, as shown in Figure 7.

The variation trend of the overall seismic reserve capacity of the abovementioned three sections is shown in Figure 8. For section R-A, when the damage index (D) ranges from 0 to 0.5, the overall seismic residual capacity is more convex than that of the curve and the attenuation rate is slow. When the damage index ranges from 0.5 to 1, the shape of the curve is concave and the attenuation rate is fast. For section R-C, the seismic residual ratio curve is approximately linear in

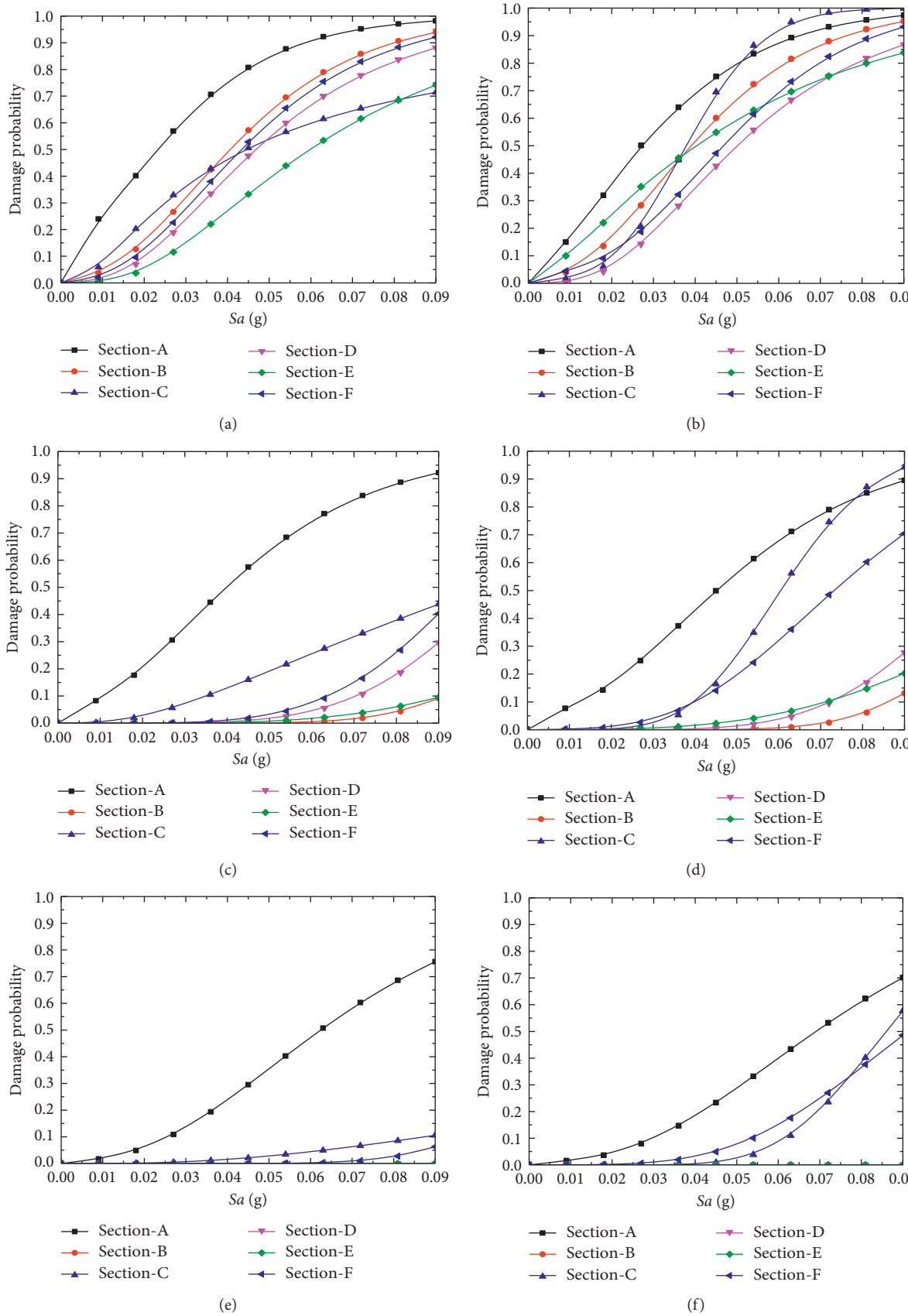

Figure 6: Continued.

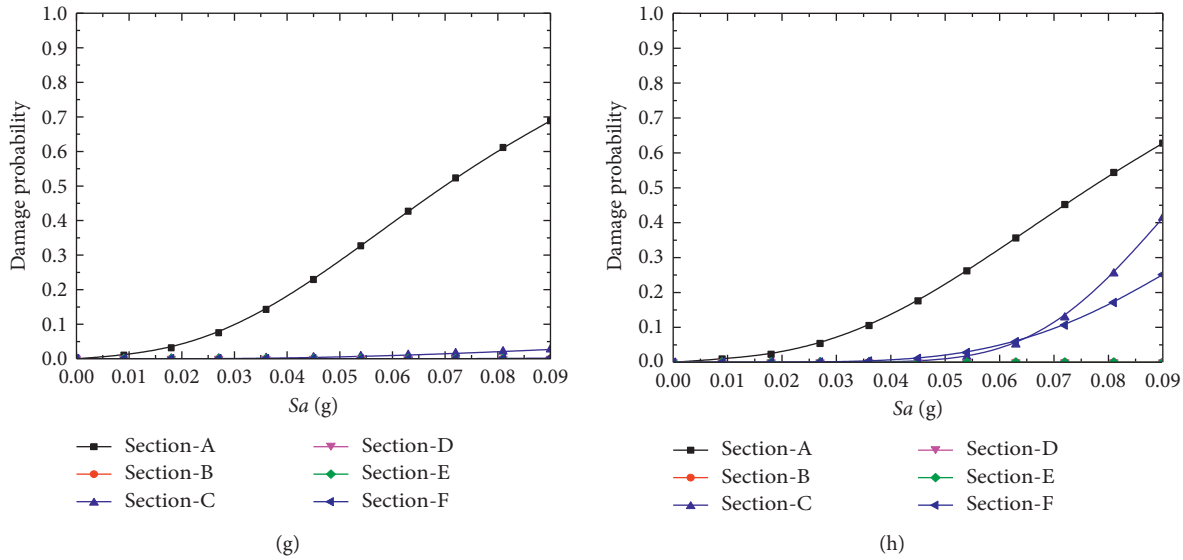

Figure 6: The fragility curves of the Puli Bridge. (a) Slight damage fragility curves of the key section of the left leg. (b) Slight damage fragility curves of the key section of the right leg. (c) Mid damage fragility curves of the key section of left leg. (d) Mid damage fragility curves of the key section of the right leg. (e) Severe damage fragility curves of the key section of the left leg. (f) Severe damage fragility curves of the key section of the right leg. (g) Complete damage fragility curves of the key section of the left leg. (h) Complete damage fragility curves of the key section of the right leg.

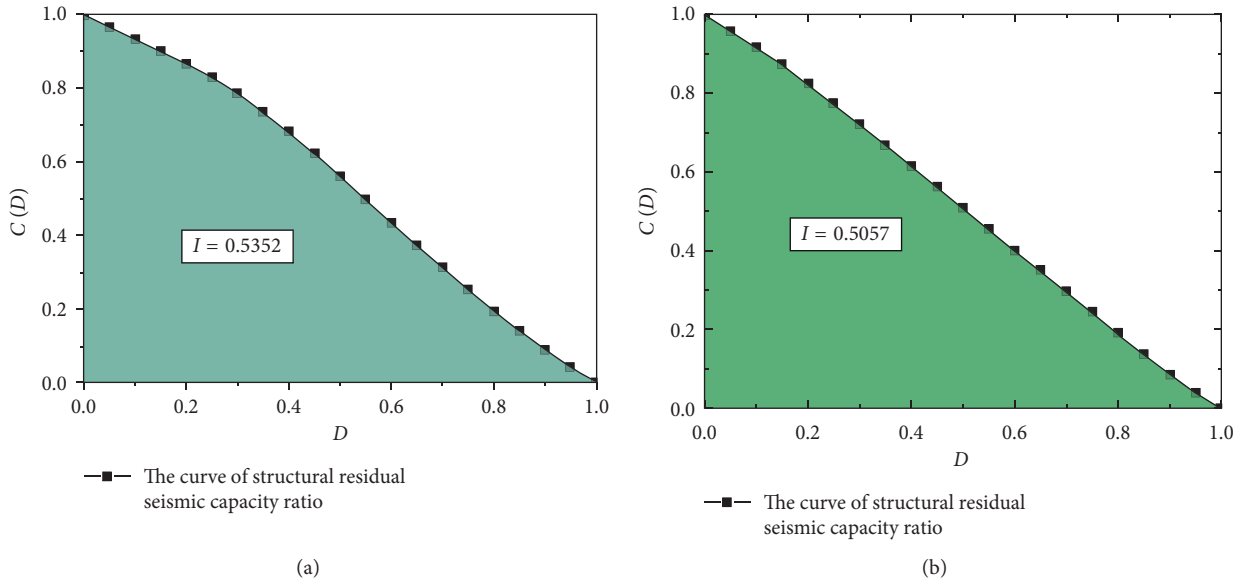

Figure 7: Continued.

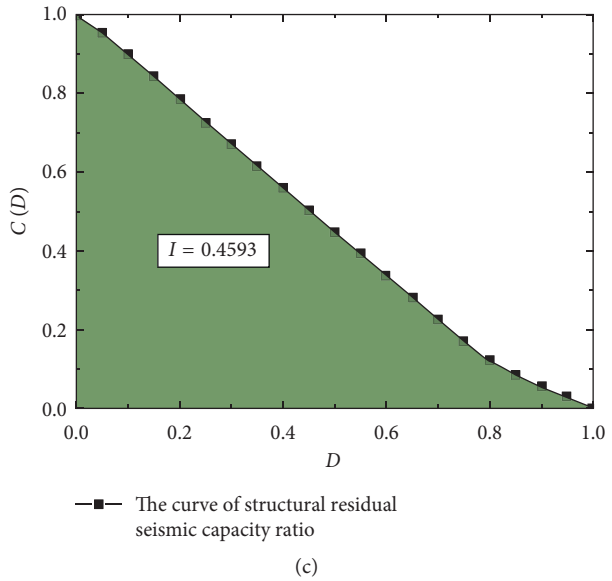

(c)

Figure 7: Residual ratio curve of the overall seismic capacity. (a) Section R-A. (b) Section R-C. (c) Section R-F.

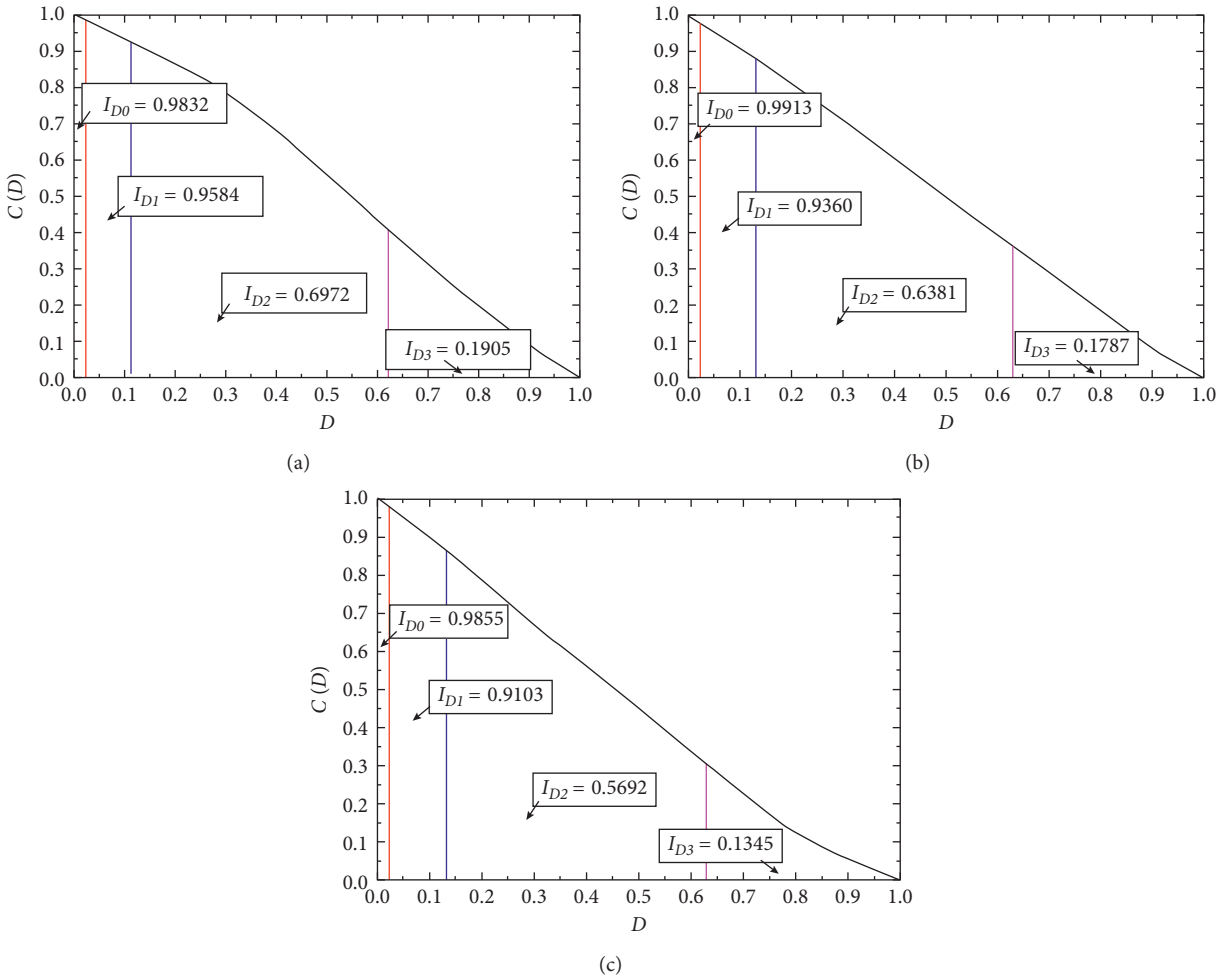

Figure 8: Residual ratio curve of stage seismic capacity. (a) Section R-A. (b) Section R-C. (c) Section R-F.

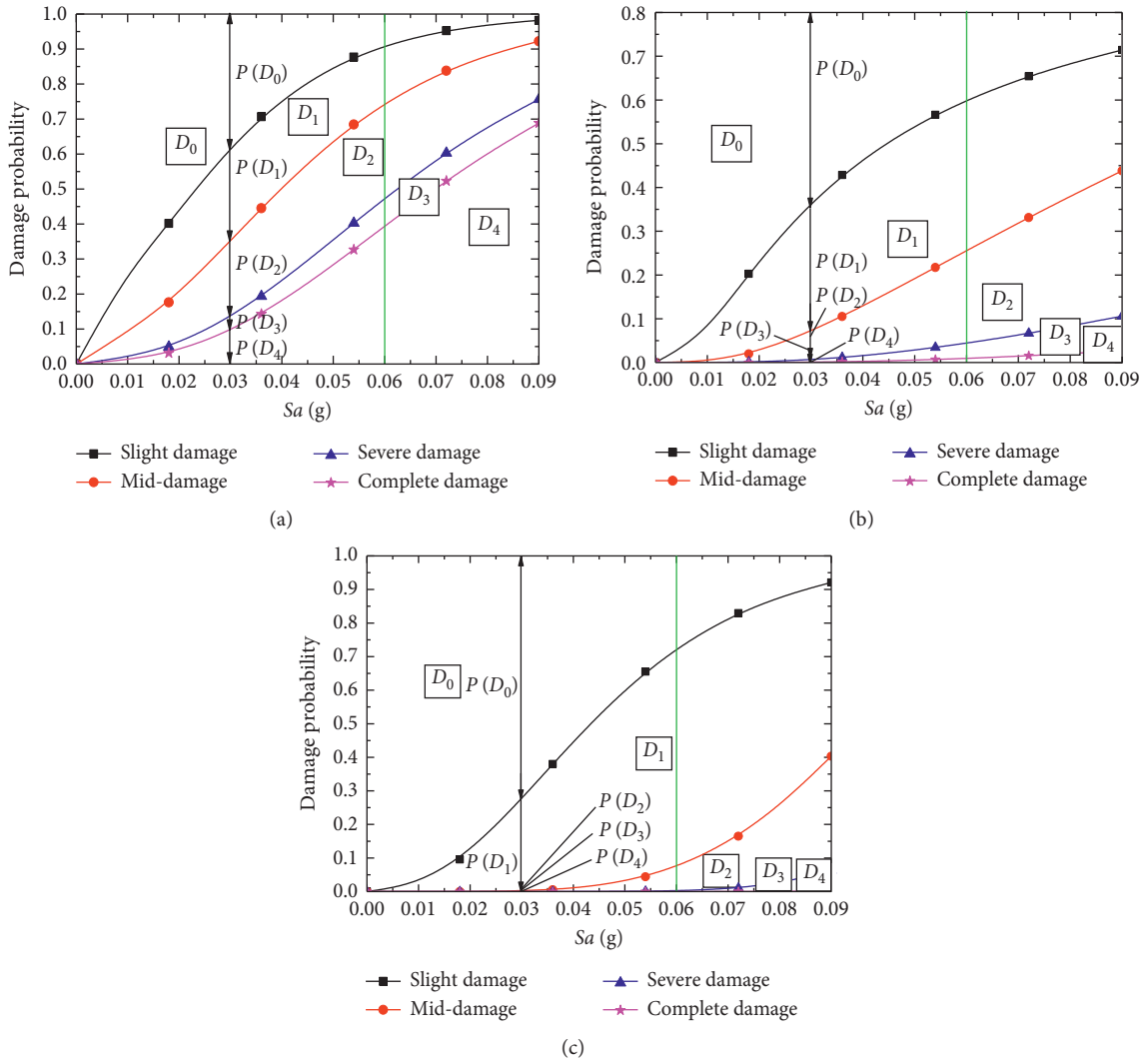

Figure 9: Different interval fragility curves. (a) Section R-A. (b) Section R-C. (c) Section R-F.

distribution and the attenuation rate is fast. For section R-F, the attenuation of the overall seismic residual capacity ratio of the damage index (D) varies linearly in the range of 0 to 0.7. When the damage index exceeds 0.7, the attenuation curve is similar to concave.

The overall recoverability index can quantitatively describe the overall seismic reserve capacity of key sections of the structure, but it cannot well obtain the seismic reserve capacity under different degrees of damage. In order to solve this problem, the ratio of seismic capacity surplus to the ultimate seismic residual ratio at each stage is defined as the stage seismic recoverability index in each damage interval. The stage recoverability of cross sections R-A, R-C, and R-F is shown in Figure 8, after the calculation.

4.4. Expected Residual Ratio of Seismic Resistance. To reflect the development law of the expected residual ratio of seismic resistance of a section under specific earthquake action, this study calculated the expected residual ratio of seismic resistance of the section for three specific ground motions: $Sa = 0.03$ g, $Sa = 0.06$ g, and $Sa = 0.09$ g, respectively, for the key sections with high damage probability.

Table 5: Seismic resilience of the stage index and damage probability (section R-A).

Damage interval	I_{Di}	$Sa = 0.03$ g	$Sa = 0.06$ g	$Sa = 0.09$ g
D_0	0.983	0.382	0.093	0.021
D_1	0.958	0.260	0.164	0.057
D_2	0.697	0.216	0.272	0.170
D_3	0.191	0.037	0.075	0.063
D_4	0	0.105	0.396	0.689

The results of the calculation of the expected residual ratio of seismic capacity under specific earthquakes are shown in Figure 9 and Tables 5–7. The results show that the seismic reserve capacity of the section has been obviously reduced under the action of ground motion and it needs to be strengthened or repaired in time.

The expected values for the given earthquake intensities could be easily estimated according to equation (5). The results are shown in Table 8.

Table 6: Seismic resilience of the stage index and damage probability (section R-C).

Damage interval	I_{Di}	$Sa = 0.03$ g	$Sa = 0.06$ g	$Sa = 0.09$ g
D_0	0.989	0.638	0.402	0.277
D_1	0.924	0.287	0.347	0.272
D_2	0.622	0.065	0.198	0.337
D_3	0.188	0.006	0.043	0.079
D_4	0	0.004	0.01	0.035

Table 7: Seismic resilience of the stage index and damage probability (section R-F).

Damage interval	I_{Di}	$Sa = 0.03$ g	$Sa = 0.06$ g	$Sa = 0.09$ g
D_0	0.9775	0.715	0.274	0.076
D_1	0.9132	0.276	0.649	0.521
D_2	0.6088	0.002	0.069	0.335
D_3	0.1828	0.002	0.002	0.056
D_4	0	0.005	0.006	0.012

where D_0, D_1, D_2, D_3, and D_4 are the damage intervals of the intact section, no damage, slight damage, mid damage, severe damage, and complete damage, respectively.

Table 8: The expected values for given earthquake intensities.

Key sections	$E_{0.03}$	$E_{0.06}$	$E_{0.09}$
Section R-A	0.7824	0.4524	0.2058
Section R-C	0.9374	0.8491	0.7495
Section R-F	0.9523	0.9028	0.7642

5. Conclusions

This study mainly focused on the residual seismic resistance and proposed a new methodology for the structure with unequal height. The proposed methodology is based on the performance of seismic fragility. The main conclusions of this study can be summarized as follows:

(1) The residual seismic capacity ratio curves of the bridge based on a large number of incremental dynamic analysis reflect the weak damage resistance of the long-span asymmetric suspension bridge, which also directly reflect the strength preparation of the bridge in the face of sequential strong earthquakes. These curves have an obvious nonlinear relationship with the damage degree and also have a great relationship with the structural system, seismic intensity index, and other factors.

(2) The results of fragility analysis show that most of the critical sections of the right arm of the main tower are in a state of severe loss. On one hand, these results support the idea that the shorter piers are obviously weaker than the higher piers. On the other hand, it also reflects the rationality of the method used in the paper.

(3) The results of integral and stage seismic resistance find that while the damage state is complete damage, the residual seismic resistance of the bridge is insufficient and it is very difficult to repair.

(4) An interesting and noteworthy phenomenon was found when we studied the residual seismic bearing capacity of short piers under specific earthquake loads. In the case of a high pier, the expected residual ratio of seismic resistance of the top is smaller than that of the bottom of the pier.

This study focuses only on the seismic residual capacity of a suspension bridge with asymmetric tall piers. More research studies are needed to investigate the effects of other structural characterizations on the seismic response and fragility analysis of bridges.

Data Availability

The data used to support the findings of this study are available from the corresponding author upon request.

Conflicts of Interest

The authors declare that they have no conflicts of interest regarding the publication of this paper.

Acknowledgments

This research was funded by projects of the National Natural Science Foundation of China (51408040), Natural Science Foundation of Shaanxi Provincial Department of Education (2017JM5110), Science and Technology Plan Project of Shaanxi Provincial Department of Communications (17-

15K), and Natural Science Research of Anhui University (KJ2019A1134).

References

[1] A. Venkittaraman and S. Banerjee, "Enhancing resilience of highway bridges through seismic retrofit," *Earthquake Engineering & Structural Dynamics*, vol. 43, no. 8, pp. 1173–1191, 2014.

[2] R. S. Hamed, M. Iman, and J. W. Hu, "Comparison of seismic reliability and risk assessment for special and intermediate steel moment frames," *KSCE Journal of Civil Engineering*, vol. 22, no. 9, pp. 3452–3461, 2018.

[3] A. Karamlou and P. Bocchini, "From component damage to system-level probabilistic restoration functions for a damaged bridge," *Journal of Infrastructure Systems*, vol. 23, no. 3, Article ID 04016042, 2016.

[4] X. L. Lv, L. M. Quan, and H. J. Jiang, "Research trend of earthquake resilient structures seen from 16WCEE," *Earthquake Engineering & Engineering Dynamics*, vol. 37, no. 3, pp. 1–9, 2017.

[5] M. Bruneau, S. E. Chang, R. T. Eguchi et al., "A framework to quantitatively assess and enhance the seismic resilience of communities," *Earthquake Spectra*, vol. 19, no. 4, pp. 733–752, 2003.

[6] X. M. Wang, P. B. Fei, and C. S. Wang, "Accelerated construction of self-Anchored suspension bridge using novel tower-girder anchorage technique," *Journal of Bridge Engineering*, vol. 24, no. 5, Article ID 05019006, 2019.

[7] L. N. Wen, Q. G. Cheng, and Q. Cheng, "Deformation experiment research on the model tunnel anchorage of Dadu River Bridge in Luding," *Journal of Railway Engineering Society*, vol. 34, no. 1, pp. 52–59, 2017.

[8] J. X. Shen, B. Liu, and L. Cui, "Structural design and global analysis of main bridge of Longjiang Bridge in Yunnan," *Bridge Construction*, vol. 44, no. 1, pp. 89–94, 2014.

[9] W. H. Tang and M. H. Chen, "Comparative study on engineering geology for site selection of Lancing River Bridge on Dali-Ruili railway," *Journal of Railway Engineering Society*, vol. 1, no. 4, pp. 8–11, 2008.

[10] F. Casciati, G. P. Cimellaro, and M. Domaneschi, "Seismic reliability of a cable-stayed bridge retrofitted with hysteretic devices," *Computers & Structures*, vol. 86, no. 17-18, pp. 1769–1781, 2008.

[11] G. Amir and K. H. Devin, "Effect of deck deterioration on overall system behavior, resilience and remaining life of composite steel girder bridges," *Journal of Bridge Engineering*, vol. 17, no. 1, pp. 623–634, 2014.

[12] B. S. Vishwanath and S. Banerjee, "Life-cycle resilience of aging bridges under earthquakes," *Journal of Bridge Engineering*, vol. 24, no. 11, Article ID 04019106, 2019.

[13] Y. Dong and D. M. Frangopol, "Risk and resilience assessment of bridges under main shock and aftershocks incorporating uncertainties," *Engineering Structures*, vol. 83, pp. 198–208, 2014.

[14] A. Decò, P. Bocchini, and D. M. Frangopol, "A probabilistic approach for the prediction of seismic resilience of bridges," *Earthquake Engineering & Structural Dynamics*, vol. 42, no. 10, pp. 1469–1487, 2013.

[15] P. Bocchini and D. M. Frangopol, "Optimal resilience and cost-based post disaster intervention prioritization for bridges along a highway segment," *Journal of Bridge Engineering*, vol. 17, no. 1, pp. 117–129, 2012.

[16] E. Alicia, E. Z. Arash, and C. Richard, "CFFT bridge columns for multihazard resilience," *Journal of Structure Engineering*, vol. 142, no. 8, Article ID C4015002, 2016.

[17] M. H. Hazus, *Multi-hazard loss estimation methodology: earthquake model hazus-MH MR5 technical manual*, PhD thesis, Federal Emergency Management Agency, Washington, DC, USA, 2010.

[18] J. B. Mander, R. P. Dhakal, N. Mashiko, and K. M. Solberg, "Incremental dynamic analysis applied to seismic financial risk assessment of bridges," *Engineering Structures*, vol. 29, no. 10, pp. 2662–2672, 2007.

[19] Q. Wang, Z. Y. Wu, and S. K. Liu, "Multivariate probabilistic seismic demand model for the bridge multidimensional fragility analysis," *KSCE Journal of Civil Engineering*, vol. 22, no. 9, pp. 3443–3451, 2018.

[20] Z. Zheng, X. L. Pan, and M. Bao, "Seismic fragility of a typical containment under bidirectional earthquake excitations," *KSCE Journal of Civil Engineering*, vol. 22, no. 11, pp. 4430–4444, 2019.

[21] W. P. S. Dias and U. Edirisooriya, "Derivation of tsunami damage curves from fragility functions," *Natural Hazards*, vol. 96, no. 3, pp. 1153–1166, 2019.

[22] T. Ucar and M. Duzgun, "Derivation of analytical fragility curves for RC buildings based on nonlinear pushover analysis," *Teknik Dergi*, vol. 24, no. 3, pp. 6421–6446, 2013.

[23] M. Bayat, F. Daneshjoo, and N. Nisticò, "The effect of different intensity measures and earthquake bayat directions on the seismic assessment of skewed highway bridges," *Earthquake Engineering and Engineering Vibration*, vol. 16, no. 1, pp. 165–179, 2017.

[24] Y. J. Park and A. H. S. Ang, "Mechanistic seismic damage model for reinforced concrete," *Journal of Structural Engineering*, vol. 111, no. 4, pp. 722–739, 1985.

[25] W. P. Wu, L. F. Li, and L. H. Wang, "Evaluation of seismic fragility of high-pier long-span bridge using incremental dynamic analysis," *Earthquake Engineering and Engineering Dynamics*, vol. 32, no. 3, pp. 117–123, 2012.

[26] Y. Chen, *Seismic fragility and resilience analysis of long-span cable-stayed bridge*, Ph.D. thesis, Chang'an University, Xi'an, China, 2018, in Chinese.

[27] C. Su, "The influence of input from synthetic ground motion field with different spatial correlation and coherency on seismic response of long-pan bridge"Ph.D. thesis, Harbin Institute of Technology, Harbin, China, 2014, in Chinese.

[28] S. E. Kim and H. T. Thai, "Nonlinear inelastic dynamic analysis of suspension bridges," *Steel Construction*, vol. 32, no. 12, pp. 3845–3856, 2010.

[29] A. Süleyman, G. Murat, A. C. Ahmet, and B. Sevim, "Construction stage analysis of humber suspension bridge," *Applied Mathematical Modelling*, vol. 36, no. 11, pp. 5492–5505, 2012.

[30] W. Xiao, Z. Wang, and H. Wei, "Seismic response analysis of self-anchored suspension bridge with multi-tower," *International Journal of Steel Structures*, vol. 16, no. 4, pp. 1329–1338, 2016.

[31] L. Sgambi, E. Garavaglia, N. Basso, and F. Bontempi, "Monte Carlo simulation for seismic analysis of a long span suspension bridge," *Engineering Structures*, vol. 78, no. 1, pp. 100–111, 2014.

[32] S. X. Zheng, X. H. Shi, H. Y. Jia, C. H. Zhao, H. L. Qu, and X. L. Shi, "Seismic response analysis of long-span and asymmetrical suspension bridges subjected to near-fault ground motion," *Engineering Failure Analysis*, vol. 115, Article ID 104615, 2020.

[33] C.-K. Jiao, X. Dong, A.-Q. Li, G.-D. Zhou, and X.-P. Wu, "Seismic response of long-span triple-tower suspension bridge under random ground motion," *Mathematical Problems in Engineering*, vol. 2017, Article ID 3457452, 16 pages, 2017.

[34] J. Martin, A. Alipour, and P. Sarkar, "Fragility surfaces for multi-hazard analysis of suspension bridges under earthquakes and microbursts," *Engineering Structures*, vol. 197, Article ID 109169, 13 pages, 2019.

[35] Y. Cheng, J. Zhang, and J. Wu, "Fragility analysis of a self-anchored suspension bridge based on structural health monitoring data," *Advances in Civil Engineering*, vol. 2019, Article ID 7467920, 19 pages, 2019.

[36] P. Franchin, F. Petrini, and F. Mollaioli, "Improved risk-targeted performance-based seismic design of reinforced concrete frame structures," *Earthquake Engineering & Structural Dynamics*, vol. 47, no. 1, pp. 49–67, 2018.

[37] S. Song, C. Qian, and Y. J. Qian, "Canonical correlation analysis of selecting optimal ground motion intensity measures for bridges," *KSCE Journal of Civil Engineering*, vol. 23, no. 7, pp. 2958–2970, 2019.

[38] N. Shome and C. A. Cornell, "Probabilistic seismic demand analysis of nonlinear structures," RMS Report 35 Reliability of Marine Structures Group, Stanford University, Stanford, CA, USA, 1999.

[39] H. Pahlavan, M. Shaianfar, G. GhodratiAmiri, and M. Pahlavan, "Probabilistic seismic fragility assessment of the structural deficiencies in Iranian in-filled RC frame structures," *Journal of Vibroengineering*, vol. 17, no. 5, pp. 2444–2454, 2015.

[40] Chinese Standard JTG/T D65-05-2015, *Specifications For Design of Highway Suspension Bridge: JTG/T D65-05-2015*, Standards Press of China, Beijing, China, 2015, in Chinese.